Geophysical Research Letters

RESEARCH LETTER
10.1029/2020GL088599

Special Section:
The Arctic: An AGU Joint Special Collection

Role of Atmospheric Variability in Driving the "Warm-Arctic, Cold-Continent" Pattern Over the North America Sector and Sea Ice Variability Over the Chukchi-Bering Sea

Weina Guan[1,2], Xianan Jiang[2,3], Xuejuan Ren[1], Gang Chen[4], and Qinghua Ding[5]

[1]CMA-NJU Joint Laboratory for Climate Prediction Studies, Institute for Climate and Global Change Research, School of Atmospheric Sciences, Nanjing University, Nanjing, China, [2]Joint Institute for Regional Earth System Science and Engineering, University of California, Los Angeles, CA, USA, [3]Jet Propulsion Laboratory, California Institute of Technology, Pasadena, CA, USA, [4]Department of Atmospheric and Oceanic Sciences, University of California, Los Angeles, CA, USA, [5]Department of Geography, and Earth Research Institute, University of California, Santa Barbara, CA, USA

Abstract While the observed decline of sea ice over the Chukchi-Bering Sea (CBS) has coincided with the "warm-Arctic, cold-continent" (WACC) pattern over the North America (NA) sector, there is a debate on the causes of the WACC pattern. Here we present a very similar WACC pattern over the NA sector on both interannual and subseasonal time scales. Lead-lag regression analyses on the shorter time scale indicate that an anomalous anticyclonic circulation over Alaska/Yukon in conjunction with the downward surface turbulent heat flux and long-wave radiation anomalies over CBS leads the formation of the WACC pattern by about 1–2 days, while the latter further leads CBS sea ice reduction by about 3 days. These results indicate that atmospheric variability may play an active role in driving both the WACC pattern over NA and CBS sea ice variability.

Key Points:
- A similar "warm-Arctic, cold-continent" (WACC) pattern is found on both interannual and subseasonal time scales over North America (NA)
- On shorter time scales, the Alaska anomalous high leads the WACC pattern by 1 to 2 days, which further leads CBS sea ice loss by about 3 days
- This study indicates that atmospheric variability plays an active role in driving the WACC pattern over NA and CBS sea ice variability

Supporting Information:
- Supporting Information S1

Correspondence to:
X. Jiang and X. Ren,
xianan@ucla.edu;
renxuej@nju.edu.cn

Citation:
Guan, W., Jiang, X., Ren, X., Chen, G., & Ding, Q. (2020). Role of atmospheric variability in driving the "warm-arctic, cold-continent" pattern over the North America sector and sea ice variability over the Chukchi-Bering sea. *Geophysical Research Letters*, *47*, e2020GL088599. https://doi.org/10.1029/2020GL088599

Received 1 MAY 2020
Accepted 29 MAY 2020
Accepted article online 4 JUN 2020

1. Introduction

Arctic has experienced rapid warming in recent decades, coincident with frequent occurrence of cold winters across mid-latitude Eurasia and North America (NA), featuring a "warm Arctic - cold continent" (WACC) pattern (e.g., Cohen et al., 2014; Kug et al., 2015; Overland et al., 2011; Screen, 2017; Sun et al., 2016). A similar WACC pattern in wintertime surface temperature anomalies has also been observed on interannual (Honda et al., 2009; Inoue et al., 2012; Mori et al., 2019; Petoukhov & Semenov, 2010; Sorokina et al., 2015) and intraseasonal time scales (Lin, 2018). While Arctic warming has generally been attributed to enhanced surface turbulent heat flux (THF) due to local sea ice loss and warmer surface water in and around the Arctic (Deser et al., 2010; Screen & Simmonds, 2010; Stroeve et al., 2007), key processes responsible for mid-latitude cold winters remain a subject of debate.

Most previous studies in understanding the WACC pattern focused on Eurasia on interannual time scales. Both observational and modeling studies suggested that harsh Eurasian winters could occur due to Arctic sea ice loss near the Barents-Kara Sea (BKS) or increased Eurasian snow cover, by inducing an anticyclonic circulation over Siberia through tropospheric Rossby wave responses (e.g., Cohen et al., 2012; Honda et al., 2009; Inoue et al., 2012; Kug et al., 2015; Mori et al., 2014; Nakamura et al., 2015; Tang et al., 2013), or through a stratospheric pathway via vertically propagating planetary waves (Cohen et al., 2014; Kim et al., 2014; Nakamura et al., 2016; Sun et al., 2015; Zhang et al., 2018).

Despite the fact that cooling anomalies over Eurasia as a response to Arctic sea ice loss is captured in several model simulations, their amplitudes are much weaker than the observed counterpart (e.g., Blackport et al., 2019; Kim et al., 2014; Mori et al., 2014; Mori et al., 2019). Moreover, a robust linkage between Arctic sea ice and Siberian wintertime cooling anomalies is not corroborated in other modeling studies (Chen et al., 2016; McCusker et al., 2016a; Ogawa et al., 2018; Sun et al., 2016). While this inconsistency among models could arise from model deficiencies in depicting sensitivity to Arctic sea ice and lack of air-sea interaction in most of the aforementioned simulations (Deser et al., 2016; Mori et al., 2019), it leads to another school of thoughts that the Siberian anticyclonic circulation that bridges Eurasian cold extremes

and Arctic warming is not directly forced by Arctic sea ice loss but instead is caused by atmospheric variability (Blackport et al., 2019; McCusker et al., 2016a, 2016b; Ogawa, 2018; Sorokina et al., 2015; Sun et al., 2016). Several recent observational studies indicate negative (downward) THF anomalies in association with reduced sea ice over BKS rather than positive THF that has been hypothesized for an active role of Arctic sea ice in driving atmospheric circulation (Blackport et al., 2019; Sorokina et al., 2015). By decomposing interactions between sea ice and atmospheric circulation on subseasonal time scales, it is illustrated that atmospheric variability can play a crucial role in driving both the WACC pattern over Eurasia and sea ice loss over BKS (Gong & Luo, 2017; Park et al., 2015; Sorokina et al., 2015).

Compared to its Eurasian counterpart, much less attention has been received in understanding the causes of the WACC pattern over the NA sector, which is independent from its Eurasian counterpart on the interannual time scale (Kug et al., 2015). While limited observations suggest that sea ice reduction over the Chukchi-Bering Sea (CBS) is closely linked to the cold NA continent (Kug et al., 2015), atmospheric variability is also proposed to be critical for both cold winters over NA and sea ice loss over CBS (Blackport et al., 2019; Sigmond & Fyfe, 2016). In this study, we aim to further elucidate the key processes responsible for cold NA winters on interannual time scales by exploring the phase relationships among several key variables involved with a similar WACC pattern on subseasonal time scales.

2. Data and Method

Monthly and daily-mean data from the ERA-Interim reanalysis (Dee et al., 2011) for the period of 1979–2017 were analyzed, including surface air temperature (SAT), sea level pressure (SLP), 10 m winds, sea ice concentration (SIC), THF (sensible plus latent heat fluxes), precipitable water (PRW), and surface downward long-wave radiation (DLWR). (For both THF and DLWR, positive values represent upward fluxes.) Since the main objective of this study is to investigate key processes regulating the wintertime WACC pattern on the interannual time scale, for both monthly and daily data, their corresponding anomalous fields were derived by removing climatological annual cycle and linear trends. Analyses in the following focus on the 38 winters from December to February.

To extract the dominant interannual variability mode of SAT and SIC over the NA sector, a singular value decomposition (SVD) analysis is conducted to decompose the covariance matrix of anomalous winter mean SAT over 20-90°N, 120°E to 60°W, and SIC over 55-75°N, 165°E to 150°W. Before the SVD analysis, SAT and SIC anomalies were weighted by the square root of the cosine of the latitude.

3. Results

Figures 1a and 1b illustrate patterns of the leading co-variability modes between winter mean SAT and SIC for the period of 1979–2017, derived by regressions of SAT and SIC anomalies against their corresponding expansion coefficients (EC_{SAT} and EC_{SIC}) of the leading SVD mode. The leading SVD mode explains 75% of the squared covariance between SAT and SIC and captures the WACC pattern in SAT anomalies with a positive center over East Siberia (ES)/Alaska and a negative center over central NA (Figure 1a), along with reduced SIC over CBS (Figure 1b). The two time series of this leading SVD mode are highly correlated on interannual time scales (Figure 1c), in agreement with previous studies that sea ice loss over CBS is closely linked to the WACC pattern over NA (Kug et al., 2015). Meanwhile, the anomalous SLP pattern derived by a similar regression onto EC_{SAT} (Figure 1a) illustrates an anomalous anticyclonic circulation over the Alaska/Yukon area, which implies advection of cold air from Arctic into central NA, and warm and moist air from the south into CBS, leading to the formation of the WACC pattern.

While a robust association between atmospheric circulation and sea ice over CBS is clearly suggested in Figure 1, how this mode is formed is difficult to be determined. One possible way is that the sea ice loss over CBS induces the anticyclonic circulation and thus the WACC pattern. An alternative interpretation could be that both CBS sea ice loss and the cooling anomalies over NA are driven by the anticyclonic circulation. If the CBS sea ice loss is expected to play an active role, a positive THF (i.e., upward from ocean to atmosphere) above sea ice loss areas should be present to drive large-scale atmospheric circulation and thus remotely induce cold anomalies over NA. Blackport et al. (2019), however, illustrated that the observed close association between CBS sea ice loss and NA cold winters are only evident when negative THF anomalies are present over CBS. This thus indicates that CBS sea ice loss results from local negative THF anomalies

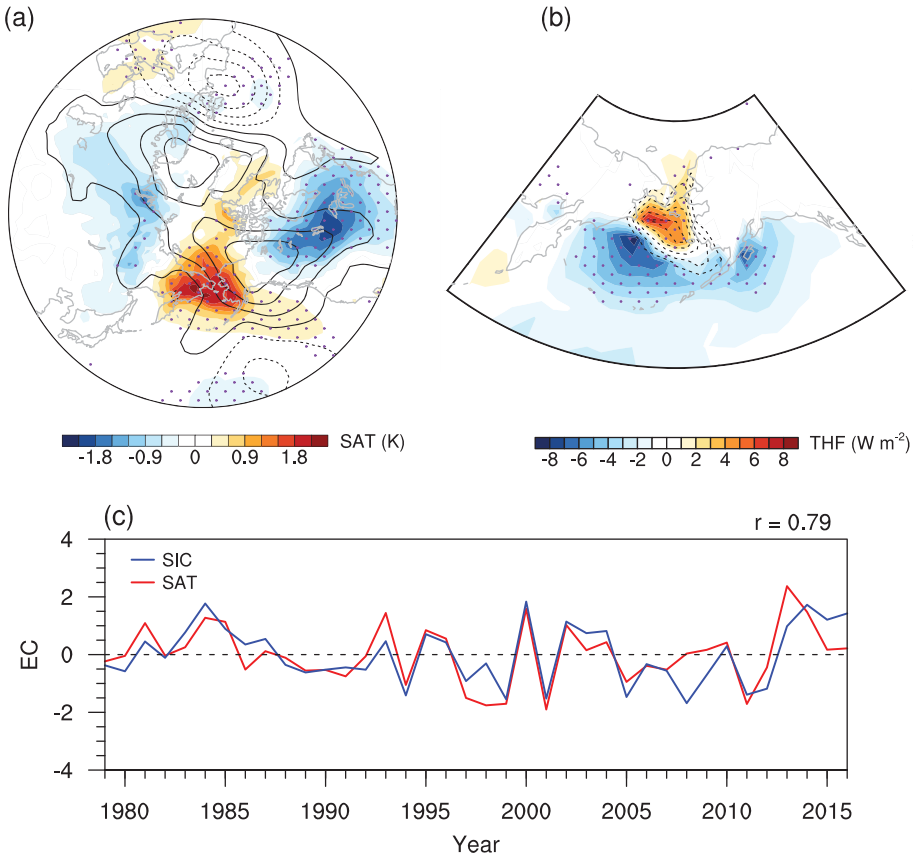

Figure 1. (a) SAT (shaded) and SLP (contours, dashed when negative; interval: 0.6 hPa), and (b) THF (shaded) and SIC (contours; interval: 3%) anomalies associated with the leading SVD mode of winter mean SAT over 20-90°N, 120°E to 60°W, and SIC over 55–75°N, 165°E to 150°W. These anomalies are derived by regressions onto EC_{SAT} and EC_{SIC} of the leading SVD mode (c). Areas with purple dots indicate shaded anomalies surpassing the 95% significance level.

driven by the overlaying atmospheric circulation, similarly as previously discussed for the Eurasian WACC pattern (Blackport et al., 2019; Sorokina et al., 2015).

To further shed light on the above processes, Figure 1b illustrates the anomalous THF pattern associated with the leading SVD mode by regression onto EC_{SIC}. A north-south dipole pattern in THF anomalies is evident over CBS. While negative THF anomalies prevail over a large area of the North Pacific and Bering Sea (NPBS) as discussed in Blackport et al. (2019), positive THF anomalies are also discerned over the reduced sea ice regions over CBS. Therefore, a potential role of CBS sea ice loss for the WACC pattern over NA cannot be completely excluded. A similar dipole signature in THF anomalies associated with Arctic sea ice loss has also been previously reported and ascribed to THF changes due to movements of the sea ice edge (e.g., Alexander et al., 2004; Deser et al., 2000; Deser et al., 2010; Sorokina et al., 2015).

Considering that the leading subseasonal SAT mode over the NA sector (Figure 2a) greatly resembles the WACC pattern associated with the interannual SAT variability in Figure 1a, the interannual variability of the WACC pattern can thus be understood by the occurrence frequency of the WACC pattern on subseasonal time scales in each winter. The direction of the causality and feedback among different fields associated with the interannual variability of the WACC pattern can be implied by exploring their evolution on subseasonal time scales (Sorokina et al., 2015).

First, in order to better understand the causality between anomalous THF and SIC associated with the WACC pattern in Figure 1b, Figure 3 presents evolution of lag-regressed THF and SIC anomalies against daily negative SIC anomalies over CBS (55–70°N, 175°E to 160°W; box in Figure 3d; using the daily SIC index projected onto the leading SVD pattern of winter mean SIC in Figure 1b yields similar results).

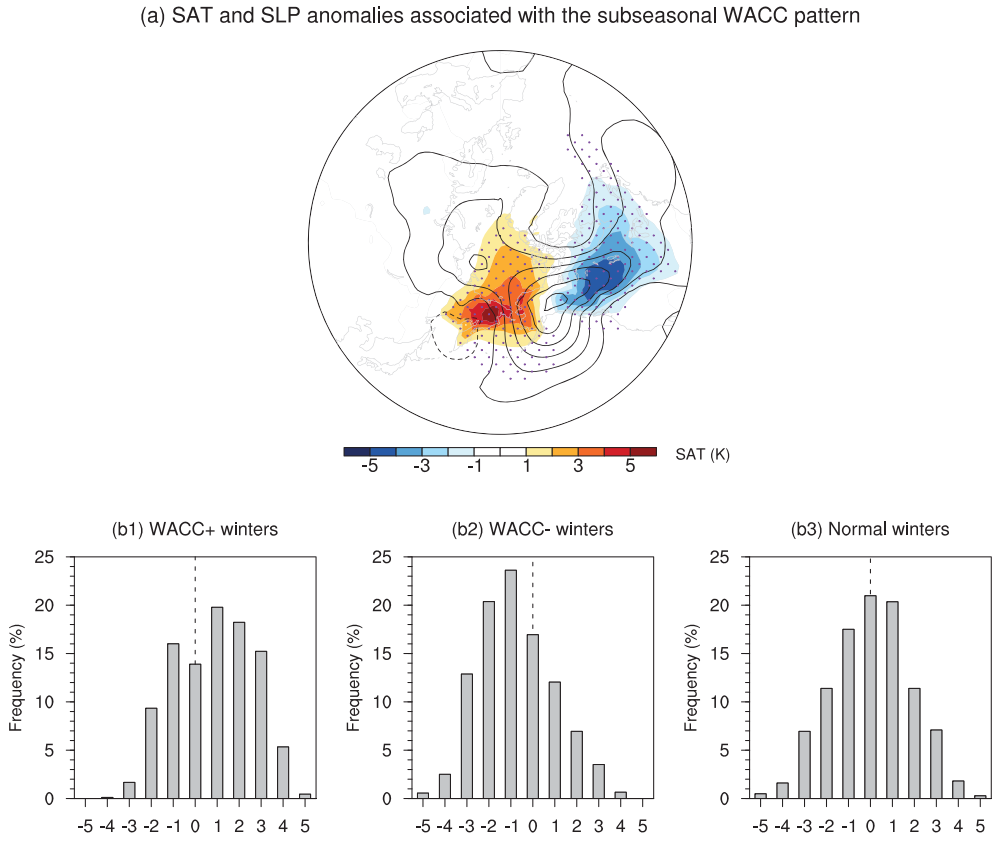

Figure 2. (a) SAT (shading; stippled for 95% significance level) and SLP (contours; interval: 1.2 hPa) anomalies associated with the leading wintertime subseasonal SAT mode over the NA sector derived by the empirical orthogonal function (EOF) analysis of daily winter SAT anomalies over 20–90°N, 120°E to 60°W. These anomalies are derived by regressions onto the principal component of EOF_1; (b) frequency distribution of daily projected WACC index onto the leading SVD pattern of SAT in Figure 1a for three groups of winters, (b1) WACC+, (b2) WACC−, and (b3) normal winters. Values in the horizontal axis in (b) represent WACC bins scaled by its standard deviation.

Large-scale negative THF anomalies, mainly confined to the south of the sea ice edge, are observed prior to the maximum sea ice reduction over CBS (i.e., Day 0). After Day 0, as negative THF anomalies to the south gradually weaken, positive THF anomalies over the reduced sea ice region become more evident, particularly at Day 10 when the negative THF signals to the south almost vanish. The large-scale negative THF anomalies before Day 0 over NPBS is mainly due to weakening of winter mean northerly winds by southerly anomalous winds associated with CBS sea ice loss (figure not shown). These results thus generally support the previous notion that CBS sea ice loss is driven by circulation-induced downward THF anomalies (Blackport et al., 2019) and prohibition of southward extension of sea ice edge by southerly wind anomalies, although the role of moisture-induced DLWR cannot be excluded as to be discussed below. Analysis on shorter time scales, however, confirms the presence of positive THF anomalies coupled with CBS sea ice loss, which could be conducive in sustaining atmospheric circulation and associated Arctic warming, although quantification of this feedback process is difficult based on observations alone. As the positive THF anomalies lag the maximum circulation anomalies, CBS sea ice loss is thus not likely to drive the circulation associated with the WACC pattern.

The close linkage between THF and large-scale circulation is further supported by the great similarity between the THF anomalies associated with the WACC pattern (Figure 1b) and the leading interannual variability mode of THF over NPBS (supporting information Figure S1a). Particularly, the anomalous SAT, SIC, and circulation patterns (Figures S1c-S1e) associated with this leading THF mode bear great resemblances to those associated with the WACC pattern in Figure 1. A significant correlation of 0.6 is found between the leading THF mode and SIC anomalies over CBS (Figure S1b).

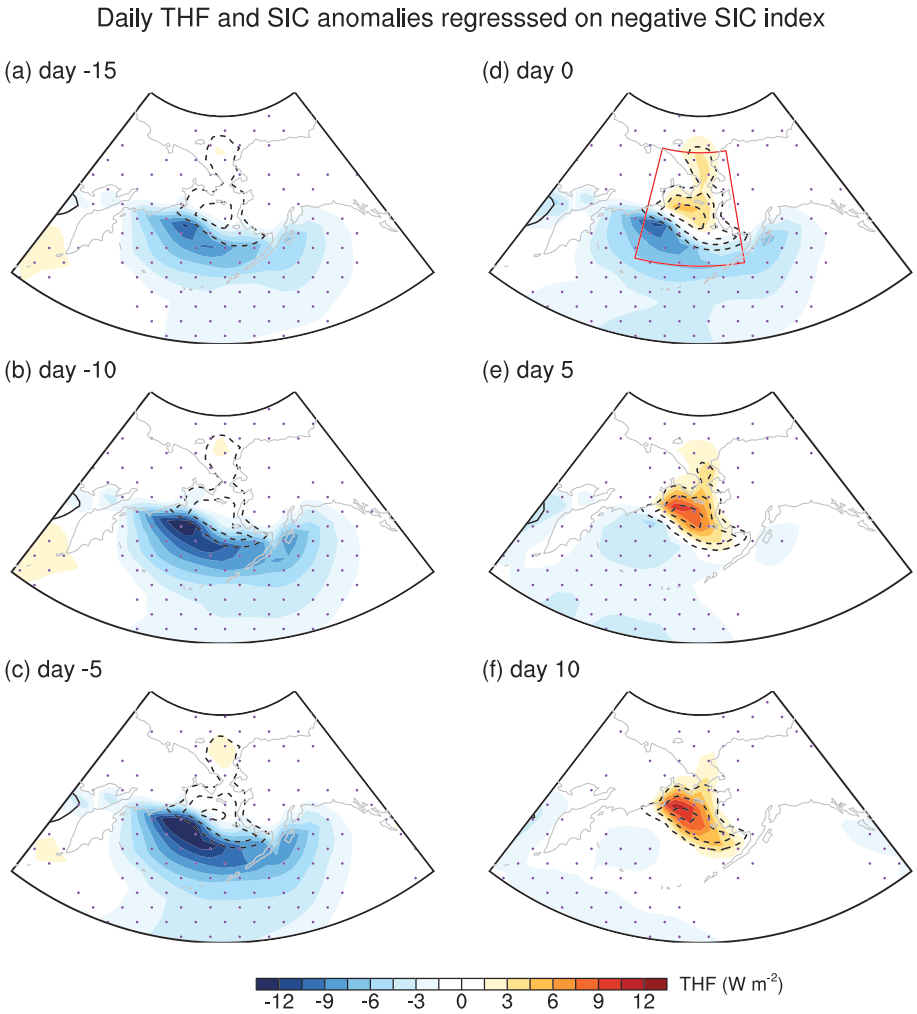

Figure 3. Lag regressions of daily THF (shading; dotted areas for 95% statistical significance level) and SIC (contours; interval: 6%, dashed if negative) anomalies onto negative daily SIC index, defined as the detrended SIC anomalies averaged over 55–70°N, 175°E to 160°W (box in d).

The causality associated with the formation of the WACC pattern over NA is further investigated by examining the lead-lag relationship among various fields on subseasonal time scales. First, we classified the 38 winters from 1979–2017 into three groups, winters corresponding to a positive phase (WACC+; $EC_{SAT} \geq 0.5$), a negative phase of the WACC (WACC−; $EC_{SAT} \leq -0.5$), and normal winters with EC_{SAT} between −0.5 and 0.5. Due to the great resemblance between the interannual and subseasonal WACC patterns as previously discussed, a daily WACC index is derived by projecting daily SAT anomalies onto the leading SVD pattern of the winter mean SAT (i.e., shaded in Figure 1a over 20-90°N, 120°E to 60°W). The advantage of this approach is that the EC_{SAT} for each winter as shown in Figure 1c can be exactly reproduced by the corresponding winter mean value of the daily WACC index. As expected, the derived daily WACC time series exhibits a prevailing spectral power on subseasonal time scales (Figure S2). Meanwhile, significantly increased occurrence of positive (negative) daily WACC events are readily seen during the WACC+ (WACC−) winters (Figure 2b).

Lead-lag regressions can then be performed for various daily anomalous fields onto the daily WACC index (Figure 4). By the method in deriving the daily WACC index, the regressed anomalous SAT pattern at Day 0 captures the WACC pattern as shown in Figure 1a, which is associated with southerly and northerly anomalous winds over CBS and central NA, respectively, accompanying with the anomalous high over Alaska/Yukon (Figure 4c), along with reduced SIC over CBS and large-scale negative THF anomalies to

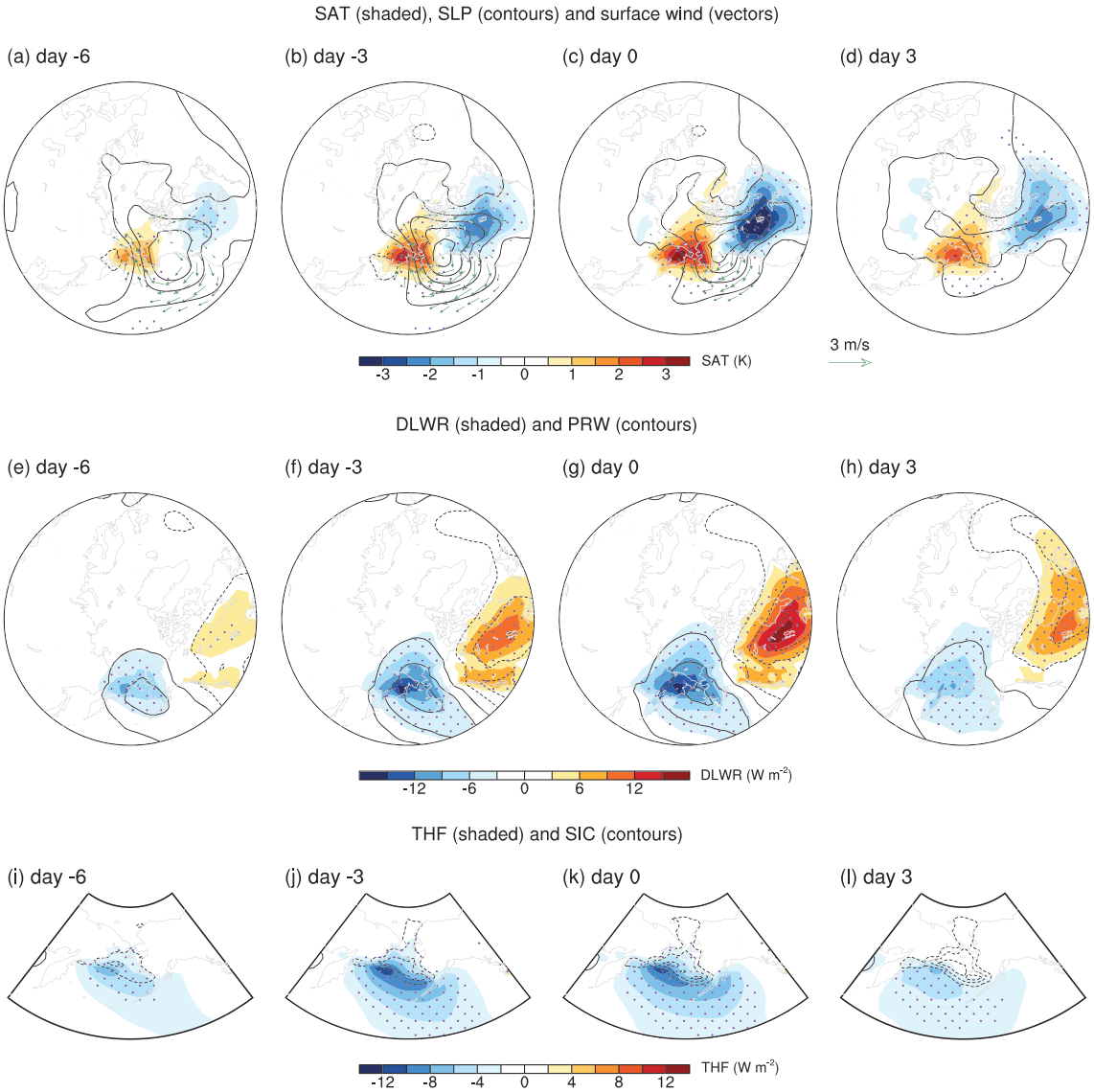

Figure 4. Lag regressions of (a–d) daily SAT (shading), SLP (contours; interval: 1.2 hPa), 10 m winds (vectors; plotted only for areas surpassing the 95% significance level); (e–h) DLWR (shading) and PRW (contours; interval: 0.3 kg·m^{-2}); (i–l) THF (shading) and SIC (contours; interval: 1.5%) onto the daily WACC index. Areas with purple dots indicate shaded anomalies surpassing the 95% significance level. Solid (dashed) contours are for positive (negative) values.

the south (Figure 4k). Additionally, the warm (cold) SAT anomalies associated with the WACC pattern are closely associated with anomalously enhanced (reduced) DLWR (Figure 4g), in agreement with previous reports on the important role of DLWR for sea ice melting (e.g., Flournoy et al., 2016; Lee et al., 2011). The enhanced (reduced) DLWR anomalies largely result from enhanced (reduced) column moisture (Figure 4g) rather than changes in clouds (not shown).

Particularly noteworthy is the phase differences among these fields on the shorter time scales. The maximum SLP anomalies and associated surface anticyclonic circulation near Alaska is observed prior to the strongest WACC pattern at Day 0, suggesting an active role of atmospheric circulation in driving the WACC pattern. Meanwhile, the maximum negative THF anomalies, enhanced PRW, and DLWR over CBS are also observed before the strongest WACC, in concert with previous discussions that both enhanced downward THF and moisture-induced DLWR anomalies can contribute to CBS warming. In contrast, the maximum CBS sea ice loss is observed after Day 0, which lags both the circulation and SAT anomalies, indicating sea ice loss as a response to local downward THF, DLWR, and warm anomalies, as well as the

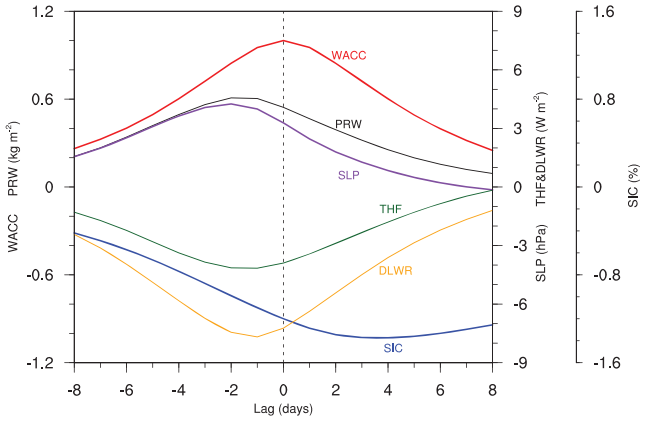

Figure 5. Evolution of the WACC index and various fields averaged over their corresponding action centers based on lag-regressions onto the daily WACC index, including SLP over Alaska/Yukon (55-70°N, 165-105°W), THF, DLWR, and PRW over NPBS (50-65°N, 160°E to 150°W), and SIC over CBS (55-70°N, 175°E to 160°W).

southerly anomalous winds that prevent its southward extension. Negative THF anomalies are largely confined to the south of the sea ice edge over NPBS as discussed in Figure 3.

The lead-lag phase relationships among the above several fields with respect to the daily WACC index are further illustrated in Figure 5 with time evolution of these variables averaged over their corresponding action centers (see figure caption for details; note that results are not sensitive to slight changes of these domains.) It is clearly illustrated that the anticyclonic circulation over Alaska/Yukon along with enhanced negative THF, PRW, and DLWR anomalies over CBS lead the WACC index by 1–2 days, while CBS sea ice reduction lags the WACC index by about 3 days. The sea ice loss over CBS, therefore, is not likely to be the initial driver of cold winters over NA associated with the WACC pattern, although it may feedback onto pre-existing atmospheric circulation anomalies as previously discussed, particularly considering its longer persistency after the peak of the WACC index (Figure 5). Note that two methodologies, one based on lead-lag regression onto daily CBS sea ice index and the other onto daily WACC index, produce similar results that atmospheric variability is the main driver of the sea ice loss over CBS. The lead-lag relationship remains unchanged even if the interannual variability in all these fields is removed. Results shown in Figures 4 and 5 are largely similar to those observed over the BKS region associated with the WACC pattern over Eurasia (e.g., Sorokina et al., 2015). The critical role of the atmospheric variability in driving both the interannual WACC pattern and CBS sea ice reduction is further supported by the lack of autocorrelations of the WACC pattern at 1 month lead/lag, and the absence of statistically significant SIC signals over CBS at 1 month lead of the WACC index (Figure S3).

4. Conclusions and Discussions

The prevailing WACC pattern of the interannual wintertime SAT variability over the NA sector is characterized by the following key processes: (i) warm anomalies over ES/Alaska and cold anomalies over central NA in association with sea ice loss over CBS; (ii) an anticyclonic circulation over Alaska/Yukon, which brings cold air from Arctic into central NA and warm and moist air from the south into CBS; (iii) a north-south dipole pattern in THF anomalies over NPBS, with positive THF anomalies over the region of reduced sea ice and negative THF anomalies to the south.

As the leading subseasonal SAT mode greatly resembles this WACC pattern, the observed interannual variability of the winter-mean WACC pattern can then be understood by a net effect of the high-frequency WACC events on subseasonal time scales. For example, a positive WACC winter is generally characterized by more frequent occurrence of positive subseasonal WACC events (Figure 2b). Lead-lag analysis on the subseasonal time scale illustrates that the anticyclonic circulation over Alaska/Yukon in conjunction with the large-scale downward THF, PRW, and DLWR anomalies over NPBS leads the WACC pattern by about 1 to 2 days, while the latter further leads sea ice reduction over CBS by about 3 days. This thus suggests that the reduced sea ice over CBS is not likely to be the initial driver of cold winters over NA associated with the WACC pattern on the interannual time scales, although sea ice loss may feedback onto pre-existing atmospheric circulation anomalies. Quantification of these detailed feedback processes, however, is not possible based on observational data sets alone and will need the aid of a coupled model that fully resolves interactions among atmosphere, land, ocean, and sea ice.

This study suggests a critical role of internal atmospheric variability, particularly on the subseasonal time scale, in driving the interannual WACC variability over the NA sector and associated sea ice loss over CBS. In order to understand and predict the climate trend and interannual variability of the WACC pattern, investigations are warranted to understand relative roles of the large-scale forcing, including the remote sea surface temperature (e.g., Sigmond & Fyfe, 2016), versus the internal atmospheric dynamics, in regulating subseasonal variability of atmospheric circulation pattern associated with the WACC pattern, that is, the anomalous surface anticyclonic circulation over Alaska/Yukon as shown in this study.

Data Availability Statement

The ERA-Interim reanalysis data were downloaded from the website (http://apps.ecmwf.int/datasets/).

Acknowledgments
WG and XR are jointly supported by the National Key Research and Development Program of China (Grant 2018YFC1505903) and the National Natural Science Foundation of China (NSFC; Grant 41621005). XJ acknowledges support by the NOAA Climate Program Office under awards NA17OAR4310261. GC is supported by NSF (Grant AGS-1832842). QD is supported by NSF Polar Programs (OPP-1744598).

References

Alexander, M. A., Bhatt, U. S., Walsh, J. E., Timlin, M. S., Miller, J. S., & Scott, J. D. (2004). The atmospheric response to realistic arctic sea ice anomalies in an AGCM during winter. *Journal of Climate*, *17*(5), 890–905. https://doi.org/10.1175/1520-0442(2004)017<0890:TARTRA>2.0.CO;2

Blackport, R., Screen, J. A., van der Wiel, K., & Bintanja, R. (2019). Minimal influence of reduced Arctic sea ice on coincident cold winters in mid-latitudes. *Nature Climate Change*, *9*(9), 697–704. https://doi.org/10.1038/s41558-019-0551-4

Chen, H. W., Zhang, F., & Alley, R. B. (2016). The robustness of midlatitude weather pattern changes due to Arctic sea ice loss. *Journal of Climate*, *29*(21), 7831–7849. https://doi.org/10.1175/jcli-d-16-0167.1

Cohen, J., Furtado, J. C., Jones, J., Barlow, M., Whittleston, D., & Entekhabi, D. (2014). Linking Siberian snow cover to precursors of stratospheric variability. *Journal of Climate*, *27*(14), 5422–5432. https://doi.org/10.1175/JCLI-D-13-00779.1

Cohen, J., Screen, J. A., Furtado, J. C., Barlow, M., Whittleston, D., Coumou, D., et al. (2014). Recent Arctic amplification and extreme mid-latitude weather. *Nature Geoscience*, *7*(9), 627–637. https://doi.org/10.1038/ngeo2234

Cohen, J. L., Furtado, J. C., Barlow, M. A., Alexeev, V. A., & Cherry, J. E. (2012). Arctic warming, increasing snow cover and widespread boreal winter cooling. *Environmental Research Letters*, *7*(1), 014007. https://doi.org/10.1088/1748-9326/7/1/014007

Dee, D. P., Uppala, S. M., Simmons, A. J., Berrisford, P., Poli, P., Kobayashi, S., et al. (2011). The ERA-Interim reanalysis: Configuration and performance of the data assimilation system. *Quarterly Journal Royal Meteorological Society*, *137*, 553–597. https://doi.org/10.1002/qj.828

Deser, C., Sun, L., Tomas, R. A., & Screen, J. (2016). Does ocean coupling matter for the northern extratropical response to projected Arctic sea ice loss? *Geophysical Research Letters*, *43*, 2149–2157. https://doi.org/10.1002/2016GL067792

Deser, C., Tomas, R., Alexander, M., & Lawrence, D. (2010). The seasonal atmospheric response to projected Arctic sea ice loss in the late twenty-first century. *Journal of Climate*, *23*, 333–351. https://doi.org/10.1175/2009JCLI3053.1

Deser, C., Walsh, J. E., & Timlin, M. S. (2000). Arctic sea ice variability in the context of recent atmospheric circulation trends. *Journal of Climate*, *13*, 617–633. https://doi.org/10.1175/1520-0442(2000)013<0617:Asivit>2.0.Co;2

Flournoy, M. D., Feldstein, S. B., Lee, S., & Clothiaux, E. E. (2016). Exploring the tropically excited Arctic warming mechanism with station data: Links between tropical convection and Arctic downward infrared radiation. *Journal of the Atmospheric Sciences*, *73*, 1143–1158. https://doi.org/10.1175/jas-d-14-0271.1

Gong, T., & Luo, D. (2017). Ural blocking as an amplifier of the Arctic sea ice decline in winter. *Journal of Climate*, *30*(7), 2639–2654. https://doi.org/10.1175/JCLI-D-16-0548.1

Honda, M., Inoue, J., & Yamane, S. (2009). Influence of low Arctic sea-ice minima on anomalously cold Eurasian winters. *Geophysical Research Letters*, *36*, L08707. https://doi.org/10.1029/2008gl037079

Inoue, J., Hori, M. E., & Takaya, K. (2012). The role of Barents Sea ice in the wintertime cyclone track and emergence of a warm-Arctic cold-Siberian anomaly. *Journal of Climate*, *25*, 2561–2568. https://doi.org/10.1175/JCLI-D-11-00449.1

Kim, B.-M., Son, S.-W., Min, S.-K., Jeong, J.-H., Kim, S.-J., Zhang, X., et al. (2014). Weakening of the stratospheric polar vortex by Arctic sea-ice loss. *Nature Communications*, *5*(1), 4646. https://doi.org/10.1038/ncomms5646

Kug, J.-S., Jeong, J.-H., Jang, Y.-S., Kim, B.-M., Folland, C. K., Min, S.-K., & Son, S.-W. (2015). Two distinct influences of Arctic warming on cold winters over North America and East Asia. *Nature Geoscience*, *8*(10), 759–762. https://doi.org/10.1038/ngeo2517

Lee, S., Gong, T., Johnson, N., Feldstein, S. B., & Pollard, D. (2011). On the possible link between tropical convection and the Northern Hemisphere Arctic surface air temperature change between 1958 and 2001. *Journal of Climate*, *24*(16), 4350–4367. https://doi.org/10.1175/2011jcli4003.1

Lin, H. (2018). Predicting the dominant patterns of subseasonal variability of wintertime surface air temperature in extratropical Northern Hemisphere. *Geophysical Research Letters*, *45*, 4381–4389. https://doi.org/10.1029/2018GL077509

McCusker, K. E., Fyfe, J. C., & Sigmond, M. (2016a). Twenty-five winters of unexpected Eurasian cooling unlikely due to Arctic sea-ice loss. *Nature Geoscience*, *9*(11), 838–842. https://doi.org/10.1038/ngeo2820

McCusker, K. E., Fyfe, J. C., & Sigmond, M. (2016b). Twenty-five winters of unexpected Eurasian cooling unlikely due to Arctic sea-ice loss. *Nature Geoscience*, *9*(11), 838–842. https://doi.org/10.1038/ngeo2820

Mori, M., Kosaka, Y., Watanabe, M., Nakamura, H., & Kimoto, M. (2019). A reconciled estimate of the influence of Arctic sea-ice loss on recent Eurasian cooling. *Nature Climate Change*, *9*(2), 123–129. https://doi.org/10.1038/s41558-018-0379-3

Mori, M., Watanabe, M., Shiogama, H., Inoue, J., & Kimoto, M. (2014). Robust Arctic sea-ice influence on the frequent Eurasian cold winters in past decades. *Nature Geoscience*, *7*, 869–873. https://doi.org/10.1038/ngeo2277

Nakamura, T., Yamazaki, K., Iwamoto, K., Honda, M., Miyoshi, Y., Ogawa, Y., et al. (2016). The stratospheric pathway for Arctic impacts on midlatitude climate. *Geophysical Research Letters*, *43*, 3494–3501. https://doi.org/10.1002/2016GL068330

Nakamura, T., Yamazaki, K., Iwamoto, K., Honda, M., Miyoshi, Y., Ogawa, Y., & Ukita, J. (2015). A negative phase shift of the winter AO/NAO due to the recent Arctic sea-ice reduction in late autumn. *Journal of Geophysical Research: Atmospheres*, *120*, 3209–3227. https://doi.org/10.1002/2014JD022848

Ogawa, F. (2018). Evaluating impacts of recent Arctic sea ice loss on the northern hemisphere winter climate change. *Geophysical Research Letters*, *45*, 3255–3263. https://doi.org/10.1002/2017GL076502

Ogawa, F., Keenlyside, N., Gao, Y., Koenigk, T., Yang, S., Suo, L., et al. (2018). Evaluating impacts of recent Arctic sea ice loss on the Northern Hemisphere winter climate change. *Geophysical Research Letters*, *45*, 3255–3263. https://doi.org/10.1002/2017GL076502

Overland, J. E., Wood, K. R., & Wang, M. (2011). Warm Arctic—Cold continents: Climate impacts of the newly open Arctic sea. *Polar Research*, *30*(1), 15787. https://doi.org/10.3402/polar.v30i0.15787

Park, D.-S. R., Lee, S., & Feldstein, S. B. (2015). Attribution of the recent winter sea ice decline over the Atlantic sector of the arctic ocean. *Journal of Climate*, *28*, 4027–4033. https://doi.org/10.1175/JCLI-D-15-0042.1

Petoukhov, V., & Semenov, V. A. (2010). A link between reduced Barents-Kara Sea ice and cold winter extremes over northern continents. *Journal of Geophysical Research*, *115*, D21111. https://doi.org/10.1029/2009jd013568

Screen, J. A. (2017). Far-flung effects of Arctic warming. *Nature Geoscience*, *10*(4), 253–254. https://doi.org/10.1038/ngeo2924

Screen, J. A., & Simmonds, I. (2010). The central role of diminishing sea ice in recent Arctic temperature amplification. *Nature*, *464*, 1334–1337. https://doi.org/10.1038/nature09051

Sigmond, M., & Fyfe, J. C. (2016). Tropical Pacific impacts on cooling North American winters. *Nature Climate Change*, *6*, 970–974. https://doi.org/10.1038/nclimate3069

Sorokina, S. A., Li, C., Wettstein, J. J., & Kvamstø, N. G. (2015). Observed atmospheric coupling between Barents Sea ice and the warm-Arctic cold-Siberian anomaly pattern. *Journal of Climate*, *29*, 495–511. https://doi.org/10.1175/JCLI-D-15-0046.1

Stroeve, J., Holland, M. M., Meier, W., Scambos, T., & Serreze, M. (2007). Arctic sea ice decline: Faster than forecast. *Geophysical Research Letters*, *34*, L09501. https://doi.org/10.1029/2007GL029703

Sun, L., Deser, C., & Tomas, R. A. (2015). Mechanisms of stratospheric and tropospheric circulation response to projected Arctic sea ice loss. *Journal of Climate*, *28*(19), 7824–7845. https://doi.org/10.1175/jcli-d-15-0169.1

Sun, L., Perlwitz, J., & Hoerling, M. (2016). What caused the recent "warm Arctic, cold continents" trend pattern in winter temperatures? *Geophysical Research Letters*, *43*, 5345–5352. https://doi.org/10.1002/2016GL069024

Tang, Q., Zhang, X., Yang, X., & Francis, J. A. (2013). Cold winter extremes in northern continents linked to Arctic sea ice loss. *Environmental Research Letters*, *8*(1), 014036. https://doi.org/10.1088/1748-9326/8/1/014036

Zhang, P., Wu, Y., Simpson, I. R., Smith, K. L., Zhang, X., De, B., & Callaghan, P. (2018). A stratospheric pathway linking a colder Siberia to Barents-Kara Sea sea ice loss. *Science Advances*, *4*, eaat6025. https://doi.org/10.1126/sciadv.aat6025